Technical University of Denmark

DTU

# Magnetic Interactions in Tb and Tb-10% Ho from Inelastic Neutron Scattering

**Bjerrum Møller, Hans; Houmann, Jens Christian Gylden; Forskningscenter Risø, Roskilde**

Link back to DTU Orbit

**DTU Library**
Technical Information Center of Denmark

## CONCLUSION

The object of this paper has been to underline the point (previously made by other authors but still often disregarded) that in the presence of orbital effects interactions are not of the Heisenberg type. Their actual form is restricted by symmetry and may be related by the above methods to microscopic models.

Detailed experimental investigation of such systems would be welcome, either from pair spectra of ions in dilute crystals from the excitation spectra in the ordered state. The low-lying excitations are spin waves and their detailed dispersion reflect the form and range of the exchange. There are also exciton bands corresponding to excitations of single-ions to higher atomic states which propagate across the crystal because of exchange. It is planned to study the theoretical form of those spectra using the more complicated spin Hamiltonians discussed above. For example $UO_2$ [17] shows signs of anisotropy which presumably arises from the exchange.

---

[17] G. Dolling and R. Cowley, Phys. Rev. Letters **16**, 683 (1966).

---

# Magnetic Interactions in Tb and Tb–10% Ho from Inelastic Neutron Scattering

H. BJERRUM MØLLER

*A.E.K. Research Establishment, Risø, Denmark*

AND

J. C. GYLDEN HOUMANN AND A. R. MACKINTOSH

*Technical University, Lyngby, Denmark*

The magnon dispersion relations and lifetimes have been measured in Tb and a Tb–10% Ho alloy by inelastic neutron scattering, in regions of both ferromagnetic and spiral ordering. In the ferromagnetic phase, the magnon energy is generally finite at zero wavevector and rises quadratically at low $q$. The magnon energies scale approximately with the magnetization. In the spiral phase the magnon energy rises linearly from zero at low $q$. The Fourier-transformed exchange parameter $J(\mathbf{q})$ has pronounced peaks in the $c$ direction, which are ascribed to transitions between states close to the Fermi surface. These peaks are less pronounced in the ferromagnetic phase. The primary mechanism limiting the magnon lifetimes appears to be interaction with the conduction electrons. In the alloy, the lifetime for magnons propagating in the $c$ direction in the ferromagnetic phase falls abruptly at about $q = 0.35$ Å$^{-1}$, and this may be due to the exchange splitting of the conduction-electron energy bands. The dispersion curve for magnons propagating in the $a$ direction is considerably perturbed around 4 meV, and this is probably due to resonant scattering on the Ho impurities. A strong coupling occurs over the same energy range in the alloy between magnons and transverse phonons propagating in the $c$ direction. This effect is considerably smaller in pure Tb.

## INTRODUCTION

The experiments described in this paper were undertaken with the aim of improving the understanding of the magnetic interactions in rare earth metals, by studying the dynamics of the magnetic systems in their ordered phases. A considerable amount of information about these interactions has been obtained from other experiments, especially from measurements of the static magnetic susceptibility[1] and neutron diffraction studies[2] of the frequently complex magnetic structures. On the other hand, the dynamical properties of the magnetic systems are a much richer source of information on the magnetic interactions than are the static properties alone, just as the study of lattice dynamics provides detailed information on interatomic

forces which a knowledge of the lattice structure alone does not.

Inelastic neutron scattering has proved to be an ideal technique for such a study, since the neutron interacts strongly with uncompensated magnetic moments, undergoing changes in energy and momentum which can readily be measured, while the scattering cross section is determined essentially by the time-dependent pair correlation function for these moments.[3] Many of the rare earth metals have undesirably high capture cross sections for thermal neutrons, but Tb is relatively favorable in this respect and has the additional advantage of a large magnetic moment, so that the magnetic scattering cross section is large. The results presented in this paper are therefore exclusively on Tb and a dilute alloy with 10% Ho, although magnetic excitations have recently been observed in Er[4]

---

[1] D. E. Hegland, S. Legvold, and F. H. Spedding, Phys. Rev. **131**, 158 (1963).

[2] W. C. Koehler, H. R. Child, E. O. Wollan, and J. W. Cable, J. Appl. Phys. **34**, 1335 (1963).

[3] L. Van Hove, Phys. Rev. **95** 1374 (1954).

[4] A. D. B. Woods, T. M. Holden, and B. M. Powell, Phys. Rev. Letters **19**, 908 (1967).

and Ho,[5] which also have reasonable neutron properties.

In the next section we describe briefly the experimental method, with especial attention to those features of the technique which allow an accurate determination of the energies and lifetimes of the magnons. The experimental results, some of which have been briefly reported previously,[6,7] are then presented. The interpretation of these data is discussed in the following section, with special reference to the relation between the conduction-electron band structure and the indirect exchange interaction between the magnetic ions. The interaction between the magnons and electrons, phonons and impurities is also considered. Finally a summary is given of the information which these experiments have provided, and plans and suggestions for future work in this field are briefly discussed.

## EXPERIMENTAL TECHNIQUE

The magnon dispersion relations and lifetimes were measured by inelastic neutron scattering, using the Risø triple axis spectrometer. The details of the experimental technique have been presented elsewhere.[8]

The scattering cross sections for one-magnon creation have the form

$$d^2\sigma/d\Omega dE \sim \sum_{\tau} (1+e_m^2)\,\delta(\kappa-\tau-\mathbf{q})\,\delta[E-\epsilon(\mathbf{q})] \quad (1)$$

for the ferromagnetic phase, and

$$d^2\sigma/d\Omega dE \sim \sum_{\tau} \{1+e_Q^2\}f^{-1}(\mathbf{q})[\delta(\kappa-\tau-\mathbf{q}-Q)$$
$$+\delta(\kappa-\tau-\mathbf{q}+Q)]+4(1-e_Q^2)f(\mathbf{q})\delta(\kappa-\tau-\mathbf{q})\}$$
$$\times\delta[E-\epsilon(\mathbf{q})] \quad (2)$$

for a spiral structure with wavevector $\mathbf{Q}$. Here $\tau$ is a reciprocal lattice vector, $\epsilon(\mathbf{q})$ is the energy of a magnon of wavevector $\mathbf{q}$, and $f(\mathbf{q})$ is a slowly varying function of $\mathbf{q}$. $\kappa=\mathbf{k}_1-\mathbf{k}_2$ is the neutron scattering vector, where $\mathbf{k}_1$ and $\mathbf{k}_2$ are the wavevectors of the incident and scattered neutrons. $e_m$ and $e_Q$ are the components of the unit scattering vector in the direction of the magnetization and spiral wavevector respectively.

The natural variables of a neutron scattering experiment are the energy transfer $E=\hbar^2/2m_0(k_1^2-k_2^2)$ and the vector $\mathbf{q}=\kappa-\tau$. The experimental method therefore consists of seeking peaks in the scattered neutron intensity by varying $\mathbf{q}$ (constant $E$ scans) or $E$ (constant $\mathbf{q}$ scans). As may be seen from the cross-section formulas, the positions of such neutron groups determine the dispersion relation $\epsilon(\mathbf{q})$, and the width of the neutron groups gives the magnon lifetimes, provided that the instrumental resolution can be extracted. Neutron groups are also produced by phonon scattering, but the cross sections in the crystals which we studied are much smaller, except at very low energy transfers. Any disturbance from phonon scattering can generally be eliminated by an appropriate choice of the relative directions of the polarization vectors and $\kappa$.

For the spiral structure, three neutron groups separated by an interval $Q$ are generally observed in a constant $E$ scan in the $c$ direction. However, if a scan is made for which $\kappa$ is along $Q$, the center peak is eliminated, so that resolution of the remaining two is easier. Figure 1 shows the results of such a constant $E$ scan for Tb–10% Ho in the spiral phase.

Because of the finite angular collimations of the neutron beam and the mosaic spread of the monochromator, sample and analyzer crystals, the variables $\mathbf{q}$ and $E$ are not sharply defined but have a distribution about their average values $\mathbf{q}_0$ and $E_0$. The probability of obtaining the values $\mathbf{q}$ and $E$ with the spectrometer set at $\mathbf{q}_0, E_0$ is defined as the resolution function $R(\mathbf{q}-\mathbf{q}_0, E-E_0)$. If the cross section is $\sigma(\mathbf{q}, E)$, we then measure the intensity

$$I(\mathbf{q}_0, E_0)=\iint \sigma(\mathbf{q}, E)\,R(\mathbf{q}-\mathbf{q}_0, E-E_0)\,d\mathbf{q}dE. \quad (3)$$

For a Bragg cross section, proportional to $\delta(\mathbf{q})\delta(E)$, we find

$$I^B(\mathbf{q}_0, E_0)\sim R(-\mathbf{q}_0, -E_0). \quad (4)$$

The resolution function can therefore be measured for $\mathbf{q}_0=0$ and $E_0=0$ by mapping the Bragg reflected intensity as a function of the spectrometer setting. Since the resolution function only depends on the distributions of $\mathbf{k}_1$ and $\mathbf{k}_2$ about their averages, it is a slowly
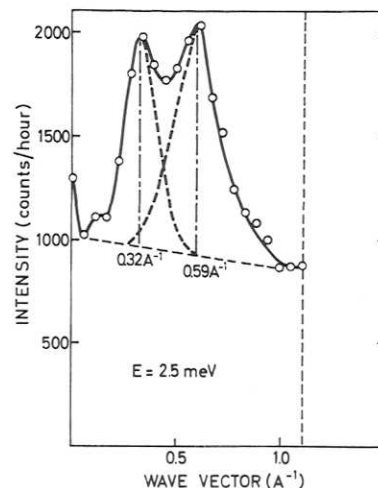


Fig. 1. Neutron groups from a constant-$E$ scan in the spiral phase of Tb-10% Ho at 200°K.

[5] H. B. Møller, J. C. G. Houmann, and A. R. Mackintosh (to be published).
[6] H. B. Møller and J. C. G. Houmann, Phys. Rev. Letters **16**, 737 (1966).
[7] H. Bjerrum Møller, J. C. G. Houmann, and A. R. Mackintosh, Phys. Rev. Letters **19**, 312 (1967).
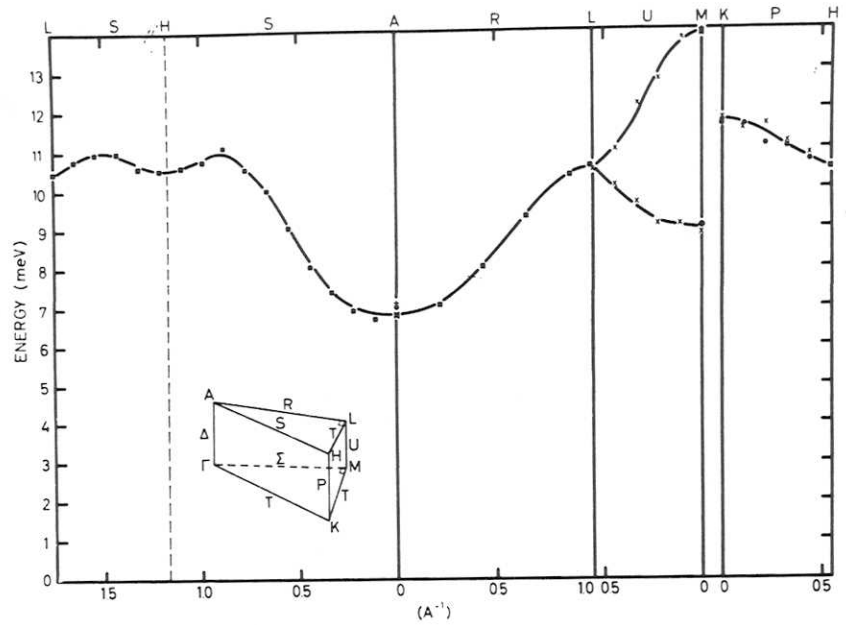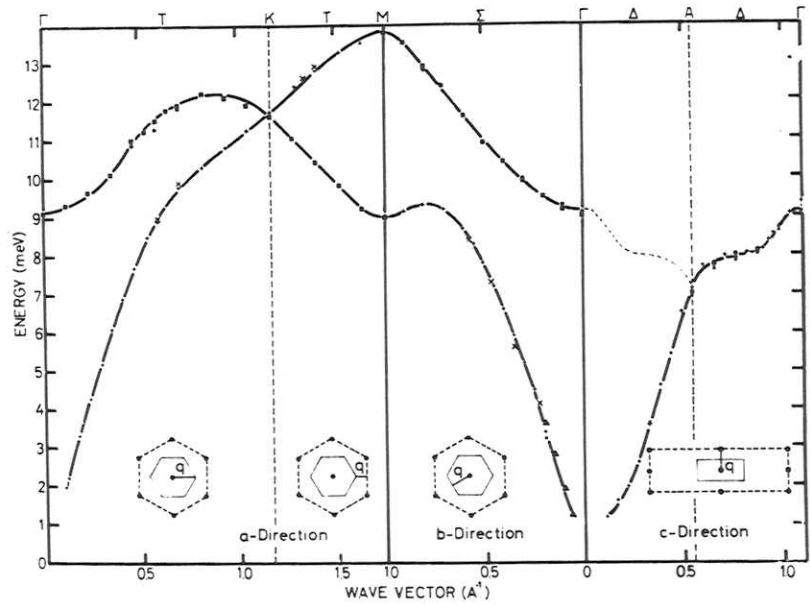[8] H. B. Møller, thesis submitted to the University of Copenhagen (1967).

FIG. 2. Experimental magnon dispersion relations in Tb along symmetry lines in the Brillouin zone at 90°K.

varying function of $q_0$ and $E_0$, so that its variation with $q_0$ and $E_0$ can be neglected when $|q_0|$ is small compared with $|k_2|$, and $E_0$ is small compared with the energy of the scattered neutrons. In this experiment, these two requirements were always fulfilled, so that the resolution function measured on a Bragg reflection was assumed to be applicable to the inelastic-scattering measurements.

There is a strong correlation between $q$ and $E$, especially when $q$ is perpendicular to $\kappa$ and in the scattering plane. This leads to focusing effects. A dispersion relation obtained with $\kappa$ perpendicular to $q$ is shown in Fig. 6, together with the half-value contour line of the resolution function. There is a strong correlation between $E$ and this component of $q$, whereas no correlation between $E$ and the other two components of $q$ was found. In a constant $q$ scan this resolution function is moved vertically and when it crosses the dispersion relation, a neutron group is observed, whose width depends on the size and orientation relative to the dispersion curve of the resolution function, and the natural width of the magnon. A knowledge of the resolution function therefore allows a determination of the resolution width for any scan. This is an important consideration when choosing scans, and in determining the natural width of the neutron groups.
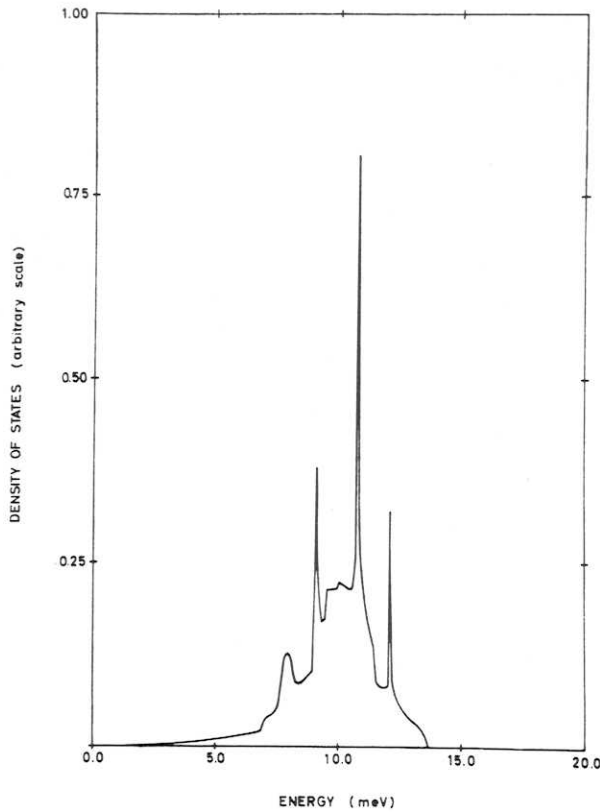
FIG. 3. Smoothed computer plot of the density of states for magnons in Tb at 90°K. The curve is normalized so that the total number of states is unity.

## EXPERIMENTAL RESULTS

The magnon dispersion relations for Tb at 90°K along all the symmetry lines in the Brillouin zone are shown in Fig. 2. The uncertainty in the measured magnon energies is estimated to be $\pm 0.1$ meV. The magnon energy is finite at $\Gamma$ and rises quadratically for small $\mathbf{q}$. The degeneracy over the hexagonal face of the zone
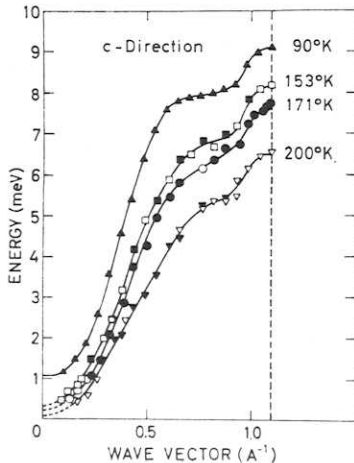


FIG. 4. Temperature dependence of magnon energies in the $c$ direction in the ferromagnetic phase of Tb.

and along the line $KH$ are consistent with the symmetry of the spin space group.[9] The kink in the dispersion curve along $\Gamma A$ is a noteworthy feature of these measurements. An analytical interpolation scheme[10] has been used to obtain magnon energies throughout the zone from the results of Fig. 2, and this method was found to give results consistent, within the experimental accuracy, with further measurements on symmetry planes and at general points within the zone. The resulting magnon density of states is shown in Fig. 3. The energy gap at $\Gamma$ and Van Hove singularities are evident in this plot.
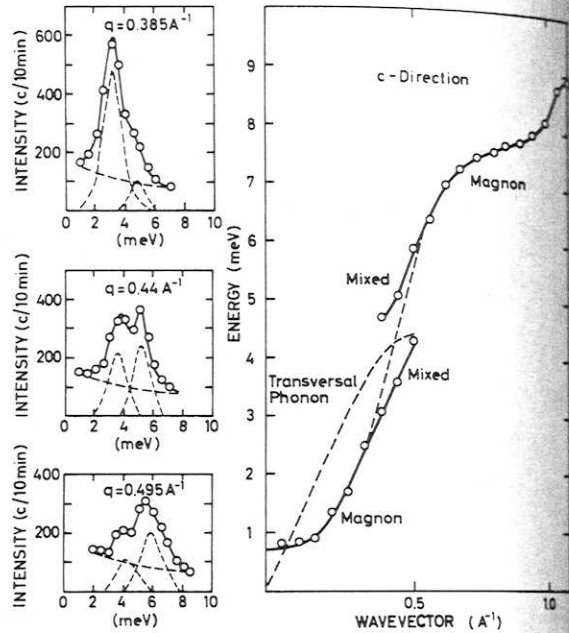


FIG. 5. Neutron groups and excitation energies in the $c$ direction of Tb–10% Ho at 110°K. The scan used for these measurements was such that transverse phonons were not observed.

The magnon energies along $\Gamma A$ have also been studied as a function of temperature in the ferromagnetic phase, and the dispersion curves in the double zone representation are shown in Fig. 4. The magnon energies decrease with temperature and the energy gap at $\Gamma$ falls rapidly to a low value.

Similar measurements in the ferromagnetic phase of a Tb–10% Ho alloy are shown in Fig. 5. The general form of the dispersion relation is similar to that in Tb, but it is rather flatter at low $\mathbf{q}$, and where it crosses the dispersion curve for the transverse phonons, there is a strong magnon–phonon coupling which causes a mixing of the modes and a splitting into two branches. The magnon–phonon interaction was also observed in pure Tb, by carefully studying the region of crossing of the

[9] W. Brinkman, J. Appl. Phys. **38**, 939 (1967).
[10] J. C. G. Houmann (to be published).

dispersion curves with good experimental resolution, and it was found to be 2–3 times smaller than in the alloy.

The magnon energies for the alloy in the $a$ direction at 110°K are shown in Fig. 6. The addition of 10% Ho to Tb causes a considerable perturbation in the dispersion relation around 4 meV, which has the form of a very rapid increase of energy over a small range of $q$. As may be seen in Fig. 2, the dispersion relation in Tb is quite linear over this range.

The natural widths of the neutron groups from magnon scattering were comparatively large, and we were able to measure them under experimental conditions such that the natural width was always substantially greater than the resolution width of the apparatus. The natural widths for magnons propagating in the $c$ direction of the alloy at 110°K decrease rather sharply at a $q$ of about 0.35 Å$^{-1}$, as shown in Fig. 7, but remain finite as $q$ goes to zero. We were unable to observe any
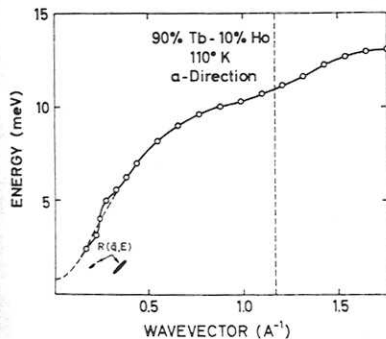


FIG. 6. Magnon dispersion relation in the $a$ direction for Tb–10% Ho at 110°K. The experimental resolution functions for the two different resolutions used are also shown.

change in the lifetime of the magnon of highest $q$ as the temperature was increased to 190°K. The magnon widths in pure Tb were also measured at small and large $q$ in the $c$ direction at 90°K, and were found to be, within the experimental error, the same as those in the alloy.

Because of the small temperature range of spiral order in Tb, it was not possible to measure the magnon dispersion relation satisfactorily in the spiral phase. The addition of 10% Ho increases the tendency towards the formation of a periodic magnetic structure however, so that the spiral phase is stable from 195° to 221°K. We were therefore able to measure the dispersion relation for magnons in the spiral phase of the alloy, and the results for the $c$ direction are shown in Fig. 8. The magnon energy rises linearly from zero at $\Gamma$ and is lower than that in the ferromagnetic phase over the whole range. The measurements at higher $q$ were difficult because of increased broadening of the neutron groups.
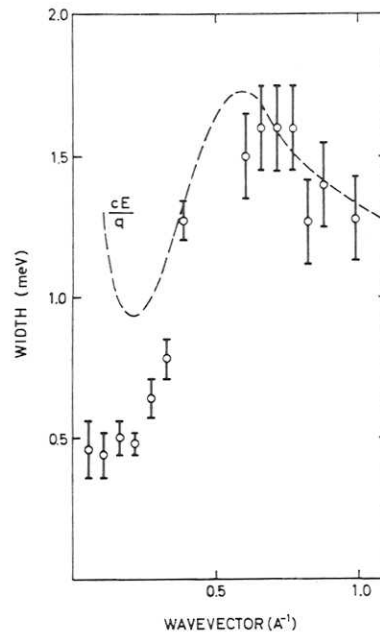


FIG. 7. Natural width of magnons propagating in the $c$ direction of Tb–10% Ho at 110°K. The experimental resolution, which is always smaller than the natural width, has been extracted from the measurements.

## DISCUSSION

In order to interpret our results, we use the simplest Hamiltonian which describes the anisotropic magnetic structures of Tb and is consistent with our measured dispersion relations. We therefore write

$$H = -\sum_{i<j} J(\mathbf{R}_i - \mathbf{R}_j)\,\mathbf{S}_i \cdot \mathbf{S}_j + \sum_j \{BS_{zj}^2$$
$$+ \tfrac{1}{2}G[(S_{xj}+iS_{yj})^6 + (S_{xj}-iS_{yj})^6]\}, \quad (5)$$

where $J(\mathbf{R}_i - \mathbf{R}_j)$ represents the indirect exchange interaction[11] between ions at $\mathbf{R}_i$ and $\mathbf{R}_j$, and $B$ and $G$
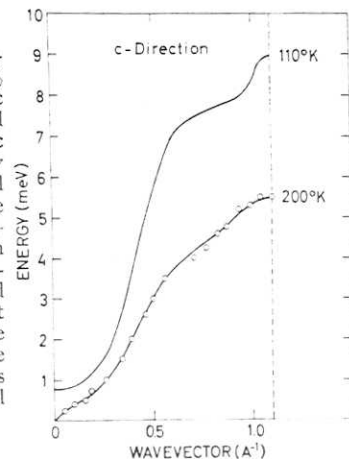


FIG. 8. Magnon dispersion relations in Tb–10% Ho in the ferromagnetic and spiral phases. The full line for the ferromagnetic phase is derived principally from the experimental points of Fig. 5, while the form of the magnon dispersion curve in the region of the magnon–phonon interaction is determined from measurements at higher temperatures. The full line for the spiral phase is a weighted least-squares fit of the experimental points to Eq. (16).

[11] M. A. Ruderman and C. Kittel, Phys. Rev. 96, 99 (1954).

FIG. 9. Fourier-transformed exchange parameters for Tb at 90°K.

are single-ion anisotropy parameters describing the twofold and sixfold anisotropy, respectively. We have used $S$ to denote the total angular momentum operator for the ions. We shall analyze the magnon dispersion relations in terms of the Fourier transforms of the indirect exchange parameters, defined by

$$J(\mathbf{q}) = \sum_{\mathbf{R}_j} J(\mathbf{R}_j) \, \exp(i\mathbf{q} \cdot \mathbf{R}_j) \qquad (6)$$
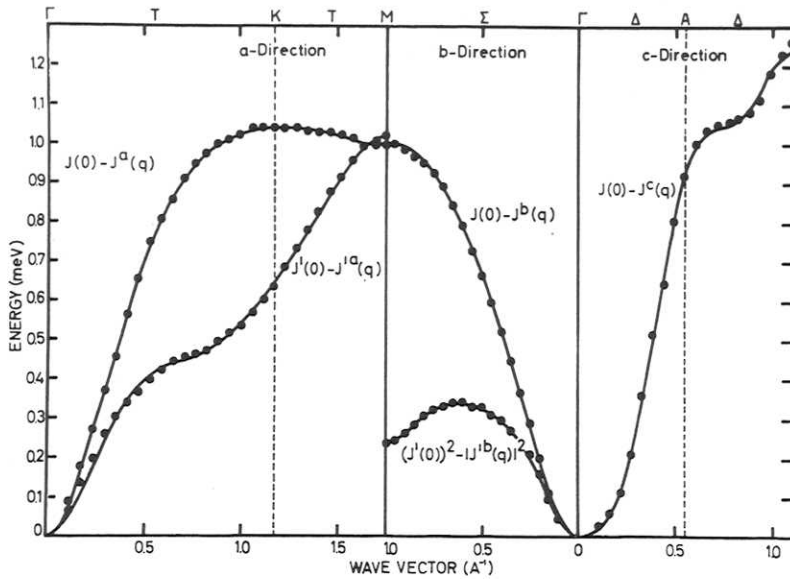
$$J'(\mathbf{q}) = \sum_{\mathbf{R}_{j'}} J(\mathbf{R}_{j'}) \, \exp(i\mathbf{q} \cdot \mathbf{R}_{j'}), \qquad (7)$$

where, in the hcp structure, unprimed vectors lie between ions in the same sublattice and primed vectors between ions in different sublattices. An approximate diagonalization of the Hamiltonian in the ferromagnetic phase[12] then gives the magnon energies

$$\epsilon_j(\mathbf{q}) = S\{ f_j^2 + 2(B + 21 G S^4) f_j + 72 G S^4 (B + 3 G S^4) \}^{1/2},$$
$$\qquad (8)$$

where

$$f_j(\mathbf{q}) = J(0) - J(\mathbf{q}) + J'(0) + (-1)^j \mid J'(\mathbf{q}) \mid \quad (9)$$

and the subscripts $j = 1$ and 2 refer, respectively, to the acoustic and optical magnon branches. For the $a$ and $b$ directions, $J(\mathbf{q})$ and $J'(\mathbf{q})$ can be written in terms of interplanar exchange parameters $J_m$ as

$$J(0) - J^a(q) = 2 \sum_{m=1}^{\infty} J_m{}^a (1 - \cos\tfrac{1}{2} m a q),$$
$$(-2\pi/a < q < 2\pi/a)$$

$$J'(0) - J'^a(q) = 2 \sum_{m=1}^{\infty} J_m{}'^a (1 - \cos\tfrac{1}{2} m a q),$$
$$(-2\pi/a < q < 2\pi/a) \quad (10)$$

_____

[12] K. Niira, Phys. Rev. **117**, 129 (1960).

and

$$J(0) - J^b(q) = 2 \sum_{m=1}^{\infty} J_m{}^b [1 - \cos(\sqrt{3}/2) \, m a q],$$
$$(-2\pi/\sqrt{3}a < q < 2\pi/\sqrt{3}a)$$

$$\mid J'(0) \mid^2 - \mid J'^b(q) \mid^2$$

$$= \sum_{m=-\infty}^{\infty} \sum_{p=1}^{\infty} J_m{}'^b J_{m-p}{}'^b [1 - \cos(\sqrt{3}/2) \, m a q],$$
$$(-2\pi/\sqrt{3}a < q < 2\pi/\sqrt{3}a). \quad (11)$$

For the $c$ direction, the ions, in the two sublattices form alternate equally separated planes and these expressions can be simplified. The dispersion relation can be considered as a single acoustical branch running to the (001) reciprocal lattice point and if, for this direction, we take the sum in Eq. (6) over all ionic sites, we have

$$\epsilon(\mathbf{q}) = S[ (J(0) - J(\mathbf{q}))^2 + 2(B + 21 G S^4)$$
$$\times (J(0) - J(\mathbf{q})) + 72 G S^4 (B + 3 G S^4)]^{1/2}. \quad (12)$$

We now require only a single set of interplanar exchange constants, such that

$$J(0) - J^c(\mathbf{q}) = 2 \sum_{m=1}^{\infty} J_m{}^c (1 - \cos\tfrac{1}{2} m c q),$$
$$(-2\pi/c < q < 2\pi/c), \quad (13)$$

where odd values of $m$ represent the exchange between planes in different sublattices.

The Fourier-transformed exchange parameters at 90°K, deduced from the average magnon energies obtained in different scans, are shown in Fig. 9. A least-squares fit of Eqs. (10), (11), and (13) to the data is also shown in Fig. 9, and the interplanar exchange parameters thus obtained are given in Table I. The

number of Fourier components used in the analysis is the minimum required to fit the data within the experimental accuracy.

The anisotropy constants used in this analysis were obtained from the neutron scattering data. $B$ was determined from the variation with $\mathbf{q}$ of the neutron group intensity in the $c$ direction. According to Lindgård et al.[13] the twofold anisotropy introduces an extra factor $(\{1+[BS/\epsilon(\mathbf{q})]^2\}^{1/2}+BS/\epsilon(\mathbf{q}))$ into the magnon scattering cross section, and from our intensities we deduce the value $B=0.25\pm0.05$ meV/ion at 110°K. From Eq. (12) the energy gap at $\Gamma$ is given by

$$S\Delta = S[72GS^4(B+3GS^4)]^{1/2}, \quad (14)$$

and from the measured energy gap at 110°K and the value of $B$ quoted above, we find $GS^4=(8.7\pm3.5)\times10^{-4}$ meV/ion. Because of the greater accuracy of the data, the measurements on the alloy were used in this analysis, but it may be assumed that the addition of 10% Ho does not drastically affect the anisotropy constants.

If we use the classical relations[12] between the macroscopic and microscopic anisotropy constants

$$K_2\simeq\tfrac{2}{3}BS^2, \qquad K_6^6\simeq GS^6, \quad (15)$$

we find quite good agreement between our value for $B$ and the value of 0.33 meV/ion deduced from torque measurements by Rhyne and Clark,[14] but our value for $G$ is about six times smaller than they obtained from magnetostriction measurements. A quantum mechanical treatment of the macroscopic anisotropy parameters,[15] taking into account the dependence of the zero-point magnon energy on magnetization, substantially modifies both Eqs. (14) and (15) however, and this may account for the discrepancy. In interpreting our result, we have therefore used the anisotropy constants

TABLE I. Interplanar exchange parameters. All are given in meV except the $J'$ for the $b$ direction, which are in meV². Accuracy ±0.005 meV.

| | $a$ direction | $b$ direction | $c$ direction |
|---|---|---|---|
| $J_1$ | 0.200 | 0.240 | 0.305 |
| $J_2$ | 0.120 | 0.040 | 0.075 |
| $J_3$ | 0.045 | 0.010 | 0.005 |
| $J_4$ | 0.020 | 0.005 | −0.035 |
| $J_5$ | 0.005 | | |
| $J_1'$ | 0.195 | 0.050 | |
| $J_2'$ | −0.005 | 0.050 | |
| $J_3'$ | 0.050 | 0.010 | |
| $J_4'$ | 0.015 | 0.010 | |
| | 0.010 | | |

[13] P. A. Lindgård, A. Kowalska, and P. Laut, J. Phys. Chem. Solids 28, 1357 (1967).
[14] J. J. Rhyne and A. E. Clark, J. Appl. Phys. 38, 1379 (1967).
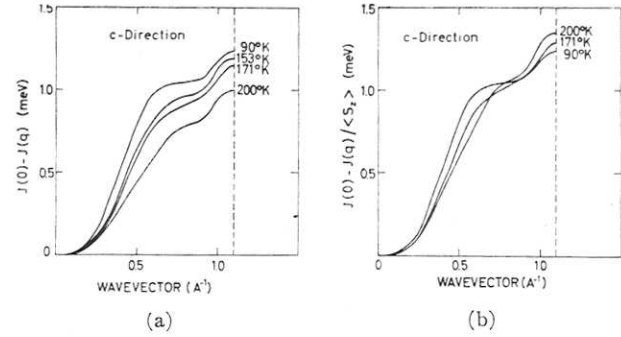[15] G. Johansen and J. R. Schrieffer (private communication).

FIG. 10. (a) Temperature dependence of the Fourier-transformed exchange parameters in the $c$ direction in the ferromagnetic phase of Tb. (b) $J(0)$-$J(\mathbf{q})$ divided by the ordered moment in the ferromagnetic phase of Tb.

derived from the neutron measurements at 110°K, but scaled with temperature according to the results of Rhyne and Clark.[14] Fortunately, the values of $J(\mathbf{q})$ deduced from the magnon dispersion curves are rather insensitive to variations in the anisotropy constants.

$J(0) - J(\mathbf{q})$ in the $c$ direction is shown as a function of temperature in the ferromagnetic phase of Tb in Fig. 10. According to the theory of Tyablikov,[16] which should be most valid at high temperatures, the exchange coupling between the ions should scale as the ordered moment, and we have therefore also plotted in Fig. 10 the function $[J(0) - J(\mathbf{q})]/\langle S_z \rangle$ for different temperatures. There is an approximate proportionality between the exchange constants and the moment, but the detailed form of $J(\mathbf{q})$ changes with temperature, and this reflects the change in energy-band structure with ordering, as well as the limitations of the theory.

A necessary condition for the stability of the spiral structure is a maximum in $J(\mathbf{q})$ at some nonzero $\mathbf{q}$, which is the wavevector $\mathbf{Q}$ of the spiral. The stronger tendency towards spiral ordering in the alloy, relative to that in pure Tb, is reflected in the flattening of the dispersion curve, and hence of $J(\mathbf{q})$ at small $\mathbf{q}$. The magnon dispersion relation in the $c$ direction in the spiral phase is[17]

$$\epsilon(\mathbf{q}) = S([J(\mathbf{Q}) - \tfrac{1}{2}J(\mathbf{Q}+\mathbf{q}) - \tfrac{1}{2}J(\mathbf{Q}-\mathbf{q})]$$
$$\times[J(\mathbf{Q}) - J(\mathbf{q})+2B])^{1/2}. \quad (16)$$

From the measured magnon energies, $J(\mathbf{q})$ can therefore be deduced by an iterative procedure, since $\mathbf{Q}$ is known from neutron-diffraction measurements, and the results which we thereby obtain are shown in Fig. 11. The incipient maxima in $J(\mathbf{q})$ in the ferromagnetic phase are developed in the spiral phase and occur around $\mathbf{Q}$ and $\boldsymbol{\tau}-\mathbf{Q}$, where $\boldsymbol{\tau}$ is the (001) reciprocal lattice vector. The condition for stability of the spiral structure is therefore satisfied.

[16] S. V. Tyablikov, Ukr. Mat. Zh. 11, 287 (1959). See also H. B. Callen, Phys. Rev. 130, 890 (1963).
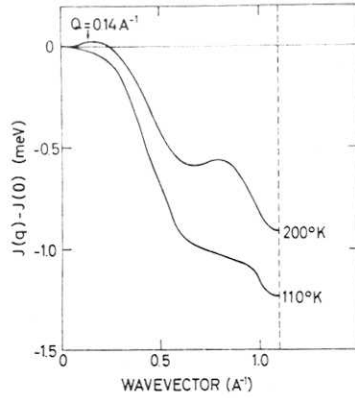[17] K. Yosida and H. Miwa, J. Appl. Phys. 32, 85 (1961).

FIG. 11. $J(\mathbf{q})$-$J(0)$ for Tb-10% Ho deduced from the dispersion curves of Fig. 8 using Eqs. (12) and (16). The dashed line is drawn at the position of the (001) reciprocal lattice point.

$J(\mathbf{q})$ is directly related to the conduction-electron energy band structure and, in the periodic zone scheme, is given by an expression of the form[18]

$$J(\mathbf{q}) = \sum_{n,n',\mathbf{k}} \frac{I_{nn'}(\mathbf{k}, \mathbf{k}+\mathbf{q})\left[ f(\epsilon_n(\mathbf{k}) - f(\epsilon_{n'}(\mathbf{k}+\mathbf{q}))\right]}{\epsilon_{n'}(\mathbf{k}+\mathbf{q}) - \epsilon_n(\mathbf{k})},$$

(17)

where $\epsilon_n(\mathbf{k})$ is the energy of a Bloch state of wavevector $\mathbf{k}$ in band $n$, $I_{nn'}(\mathbf{k}, \mathbf{k}+\mathbf{q})$ is a slowly varying function and $f(\epsilon)$ is the Fermi–Dirac distribution. The peaks in $J(\mathbf{q})$ probably reflect the contributions of a large number of small-energy denominators at $\mathbf{q}$ values corresponding to the separation between approximately parallel sheets of the Fermi surface. These are believed to be of primary importance in determining $\mathbf{Q}$ in the heavy rare earth metals.[1,s] Measurements at intermediate temperatures show that these peaks are abruptly flattened at the ferromagnetic transition, and this may be ascribed to the splitting of the different spin bands by the ferromagnetic exchange interaction.

The energy eigenvalues for the conduction electrons in Tb have been calculated along symmetry lines in the Brillouin zone by the RAPW method,[20] and part of the band structure is shown in Fig. 12. The energy bands are qualitatively similar to those in the other hcp rare earth metals, except that the $d$ bands are substantially lower in energy than those in, for instance, Dy.[21] The position of the second lowest doubly degenerate level at $L$ relative to the Fermi level is believed to be of great importance in determining the magnetic ordering in these metals. In most of them it lies above the Fermi level, but in Gd it is below and this is believed to modify the Fermi surface in such a way that $J(\mathbf{q})$ has a maximum at $\mathbf{q}=0$, resulting in a stable ferromagnetic structure. This level is also below the Fermi

level in Tb, and this may partially account for the strong tendency towards ferromagnetism, and the anomalously small $\mathbf{Q}$ in the spiral phase.

Since the neutron group widths are neither observably temperature dependent at high $\mathbf{q}$ nor significantly different in the alloy from those in pure Tb, the principal mechanism limiting the magnon lifetime is probably absorption by the conduction electrons.[22] This process involves a spin-flip by the electron, and the absorption may therefore decrease rapidly at critical wavevectors determined by the separation of the Fermi surfaces of different spin. For the free-electron model, the width well above the critical $\mathbf{q}$ is given by[22]

$$\Delta\epsilon(\mathbf{q}) = c\epsilon(\mathbf{q})/q,$$

(18)

where $c$ is a constant. This function, fitted at $q=0.72$ Å$^{-1}$ is shown in Fig. 7. The rapid fall in the widths at about $q=0.35$ Å$^{-1}$ may reflect the exchange splitting of the Fermi surface, and it would clearly be of interest to study this phenomenon as a function of magnetic ordering. The residual broadening at low $\mathbf{q}$ is probably due to Umklapp processes of the type discussed by Luther and Tanaka.[23]

Because of their smaller spin, the Ho moments in the alloy are coupled comparatively weakly to the Tb host moments and so have a natural precession frequency in the band of magnon energies. The resonant scattering of the magnons by the impurities causes a strong perturbation of the dispersion relation in the vicinity of this frequency, and this probably explains the anomaly which is shown in Fig. 6. This resonant magnon mode is discussed in more detail elsewhere.[24]

Finally we discuss the magnon–phonon interaction, which is observed when the unperturbed magnon and transverse phonon dispersion curves cross. If a linear coupling between the excitations is assumed, the Hamil-
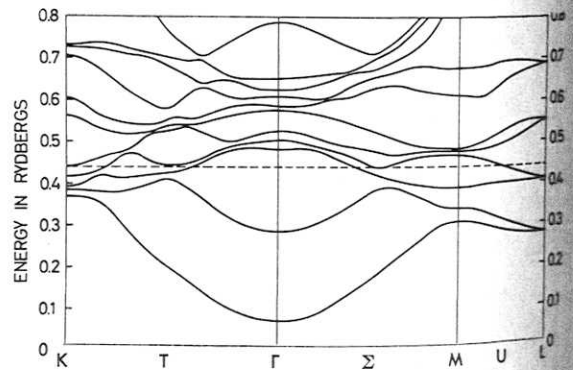


FIG. 12. Conduction-electron energy bands along symmetry directions in Tb. The dashed line is the approximate Fermi level.

[18] L. M. Roth, H. J. Zeiger, and T. A. Kaplan, Phys. Rev. 149, 519 (1966).
[19] R. W. Williams, T. L. Loucks, and A. R. Mackintosh, Phys. Rev. Letters 16, 168 (1966).
[20] T. L. Loucks, Phys. Rev. 139, A1333 (1965).
[21] S. C. Keeton and T. L. Loucks, Phys. Rev. (to be published).

[22] R. J. Elliott and H. Stern, Inelastic Scattering of Neutrons (IEAE, Vienna, 1961).
[23] A. H. Luther and T. Tanaka (to be published).
[24] A. R. Mackintosh and H. B. Møller, Proceedings of Localized Excitations Conference, Irvine, California, 1967 (to be published).

tonian may be written in the form[25]

$$H = \sum_q [\epsilon^m(\mathbf{q}) a_q^+ a_q + \epsilon^p(\mathbf{q}) b_q^+ b_q + c_q(a_q^+ b_q + a_q b_q^+)],$$

(19)

where $a_q$ and $b_q$ are destruction operators for magnons and phonons, respectively. This Hamiltonian may be diagonalized to yield eigenstates which are mixtures of spin deviation and lattice displacement, and the spin deviation part of the excitations is observed in the scan of Fig. 5. The dispersion curves split about the crossing point of the unperturbed dispersion relations, and the splitting at this point is $2c_q$. From our measurements on the alloy we therefore find that the coupling parameter $c_q$ is 0.85 meV at $\mathbf{q}=0.44$ Å$^{-1}$, which is comparable in magnitude with the value observed in $UO_2$ by Dolling and Cowley.[26] The interaction is considerably weaker in pure Tb and furthermore there is no observable coupling in the alloy between magnons and phonons propagating in the $a$ direction, for which the crossing occurs at much higher energy. It seems possible, therefore, that the coupling is enhanced by the large spin and charge deviations occurring around the Ho impurities near the resonance frequency which, fortuitously, is close to the crossing point of the magnon and phonon dispersion curves.

## CONCLUSIONS

From our measurements of the magnon dispersion relations we have been able to obtain a considerable amount of information about the magnetic interactions in the heavy rare earth metals. The indirect exchange coupling between the ions has been studied under various experimental conditions, and its form can be related to the Fermi surface. The temperature dependence reflects the effect of the change in the ordered moment on the magnon energies and on the conduction electron energy bands. The exchange splitting of the energy bands is also manifested in the magnon lifetimes, since the interaction of magnons with conduction electrons apparently drops rather rapidly at a critical $\mathbf{q}$ determined by this splitting. The resonant scattering of the magnons from Ho impurities produces a pronounced anomaly in the dispersion relation. A strong coupling occurs between magnons and transverse phonons propagating in the $c$ direction, which may be enhanced by the presence of the resonance.

There are a number of extensions, both experimental and theoretical, which could be made to this work. A more detailed study of the magnon energies and lifetimes as a function of temperature would provide further information on the relation between the conduction electrons and the magnetic interactions. In particular, a study of the magnon energies in the spiral phase should show the effect of the progressive modification of the energy bands by the magnetic ordering, and this should also be reflected in the magnon lifetimes in the ferromagnetic phase, which are critically dependent on the exchange splitting of the bands. From the conduction-electron energy bands, it should be possible to calculate both the exchange coupling between the magnetic ions and the damping of the magnons through absorption by the conduction electrons.

The change in magnon energies with magnetic ordering, and hence with temperature, should allow a more detailed study of the energy of the resonant mode and the strength of the magnon–phonon coupling as a function of $\mathbf{q}$. We are planning soon to extend our measurements down to liquid He temperatures.

It should also be possible to make detailed measurements on other rare earth metals and alloys in different magnetically ordered phases. Preliminary measurements have already been made on Er[4] and Ho.[5] We expect that the maxima in $J(\mathbf{q})$ are more pronounced in these metals, since they form periodic magnetic structures over the whole temperature range of ordering. Such experiments, together with theoretical studies of the magnetic interactions, should substantially improve our understanding of magnetism in the rare earth metals.

[25] C. Kittel, *Quantum Theory of Solids*, (John Wiley & Sons, Inc., New York, 1963), p. 74.
[26] G. Dolling and R. A. Cowley, Phys. Rev. Letters **16**, 683 (1966).